JOURNAL OF GUIDANCE, CONTROL, AND DYNAMICS
Vol. 32, No. 3, May–June 2009

Analytical Model to Find Frozen Orbits for a Lunar Orbiter

A. Abad,* A. Elipe,† and E. Tresaco‡
Universidad de Zaragoza, 50009 Zaragoza, Spain

DOI: 10.2514/1.38350

Analytical theories based on Lie–Deprit transforms are used to obtain families of periodic orbits for the problem of an orbiter around the moon. Low and moderately high orbit models are analyzed. Equilibria of the normalized equations of motion provide the representation of a global portrait of families of frozen orbits depending on values of the inclination, eccentricity, and semimajor axis. By means of the inverse transformation it is possible to refine the initial conditions for frozen orbits of a simplified model, and these initial conditions may be used as starters of numerical continuation methods when more complex models are considered.

I. Introduction

THE problem of finding periodic orbits about the moon, natural satellites, or asteroids is of current interest because several space missions have the goal of orbiting around such bodies (see for instance [1–6] and references therein). Among the possible orbits, frozen orbits are especially useful; indeed, frozen orbits are characterized by having constant eccentricity, inclination, and pericenter direction on the average, thus, they are very convenient for reconnaissance and science missions. Several procedures are used to find frozen orbits, from brute force, that is, by zeroing Gauss equations and solving the corresponding system, to more sophisticated methods like the grid method [7], by Poincaré sections [8], by numerical continuation of families of periodic orbits [9], or by averaging the Hamiltonian and finding the equilibria of the reduced Hamiltonian. This last procedure is the one that we will use in this work; it has been successfully used for finding frozen orbits for the zonal problem of an Earth artificial satellite [10,11] and to get insights on the so-called *critical inclination* [12].

In general, for orbiters around the moon, it is necessary to consider the third-body attraction, that is, the Earth's attraction, which means that time explicitly appears in the Hamiltonian. However, due to the 1:1 resonance of the moon, we can circumvent this difficulty by formulating the problem in a synodic frame rotating with the Earth, which is assumed to move on a circular orbit about the moon. The penalty we must pay is the addition of a new term in the Hamiltonian due to the Coriolis effect. Thus, we deal with a Hamiltonian characterized by the Kepler problem, the moon's gravitational potential, the Coriolis term, and the third-body attraction. A thorough analysis is needed concerning the contribution of each term and their differences, as well as how we can scale the Hamiltonian. We shall see that the scaling strongly depends on the altitude of the orbits, in such a way that for low orbit altitudes the influence of the third body is almost negligible and, consequently, we may approach this problem using the zonal problem. However, for moderate altitudes we need to cope with all four terms. We give a brief description on the Lie–Deprit transform used in our work, namely, the Delaunay normalization (Sec. III). The analytical integration is done (by means of the symbolic-numeric environment *MathATESAT* [13]) for both cases, low- and moderate-altitude orbits (Sec. IV). Let us stress that we are not interested in obtaining a complete analytical theory (as for instance those generated by de Saedeleer and Henrard [14,15]) nor in the generation of ephemerides, but to help in mission designing, where frozen orbits are of major interest; this is the main reason for including in the potential function only the zonal terms J_2 and J_7. Once the analytical integration is made, we find a global picture of families of frozen orbits, depending on three parameters: inclination, eccentricity, and semimajor axis, which allows us the obtaining of approximate frozen orbits for low (Sec. V) and moderate (Sec. VI) altitudes. These almost-frozen orbits can be used as starters of a corrector procedure [16] to get frozen orbits (Sec. VII) when more terms are included in the problem.

II. Dynamical Model

We consider the motion of an orbiter about the moon under its gravitational force and the third-body attraction due to the Earth under the Hill hypothesis, that is, the moon is in circular orbit about the Earth and the orbiter in synchronization with the rotation of the moon.

Let us consider a rotating reference frame $Oxyz$, centered on the moon and such that the plane Oxy coincides with the moon's equator and the Ox axis continuously points towards the Earth, which moves in a circular orbit with radius a_e synchronized with the rotation of the moon. Let $\boldsymbol{\omega}$ be the angular velocity vector of the moon; thus, the Hamiltonian is

$$\mathcal{H} = \frac{1}{2}\boldsymbol{X}\cdot\boldsymbol{X} - \boldsymbol{\omega}\cdot(\boldsymbol{x}\times\boldsymbol{X}) + V_M + V_E$$

were V_M and V_E are the gravitational potentials of the moon and Earth, respectively.

For the moon we only take into account the zonal contribution, thus

$$V_M = -\frac{\mu}{r} + \frac{\mu}{r}\sum_{n\geq 2}\frac{\alpha}{r}J_n P_n(z/r)$$

with α the equatorial radius of the moon, $r = \|\boldsymbol{x}\|$ the radial distance, μ the Gaussian constant for the moon, J_n the moon harmonics coefficients, and P_n the Legendre polynomial of degree n.

The gravitational potential created by the Earth is (e.g., [17])

$$V_E = -\mu_e\left(\frac{1}{\|\boldsymbol{x}_e - \boldsymbol{x}\|} - \frac{\boldsymbol{x}_e\cdot\boldsymbol{x}}{\|\boldsymbol{x}_e\|^3}\right) \tag{1}$$

where $\mu_e = \mathcal{G}m_e$, and because the orbit of the Earth is assumed to be circular, $\mu_e = \mathcal{G}m_e$ may be represented as $\mu_e = \omega^2 a_e^3$.

Presented as Paper 184 at the 18th AAS/AIAA Space Flight Mechanics Meeting, Galveston, TX, 27–31 January 2008; received 1 May 2008; revision received 19 October 2008; accepted for publication 3 November 2008.

*Associate Professor, Grupo de Mecánica Espacial, Instituto Universitario de Matematicas y Aplicaciones.

†Professor, Grupo de Mecánica Espacial, Instituto Universitario de Matematicas y Aplicaciones. Associate Fellow AIAA.

‡Ph.D. Student, Grupo de Mecánica Espacial, Instituto Universitario de Matematicas y Aplicaciones.

The first summand of this expression may be expanded as a series of Legendre polynomials as

$$\frac{\mu_e}{\|\boldsymbol{x}_e-\boldsymbol{x}\|}=\frac{\mu_e}{a_e}\left[1+\left(\frac{r}{a_e}\right)^2-2\frac{r}{a_e}\cos\beta\right]^{-1/2}$$
$$=\frac{\mu_e}{a_e}\sum_{n\geq 0}\left(\frac{r}{a_e}\right)^n P_n(\cos\beta) \tag{2}$$

with $\cos\beta=\boldsymbol{x}_e\cdot\boldsymbol{x}/ra_e=x/r$.

Legendre polynomials are

$$P_0(\cos\beta)=1,\qquad P_1(\cos\beta)=\cos\beta$$
$$P_2(\cos\beta)=(-1+3\cos\beta)/2,\ldots$$

Note that the term containing P_0 is constant, whereas the second summand of Eq. (1) cancels with the term P_1.

Because Legendre polynomials are bounded functions ($|P_n(x)|\leq 1,\ \forall\ x\in[-1,1]$), every term in Eq. (2) is bounded by $\omega^2r^2(r/a_e)^{n-2}$, thus and because $r\ll a_e$, we shall take only into consideration terms up to P_2, hence, the attraction of the third body is simply

$$V_E=\frac{\omega^2}{2}(r^2-3x^2)$$

Consequently, the Hamiltonian of the orbiter may be split into the sum

$$\mathcal{H}=\mathcal{H}_K+\mathcal{H}_C+\mathcal{H}_Z+\mathcal{H}_{3b} \tag{3}$$

where $\mathcal{H}_K$ corresponds to the Kepler problem, $\mathcal{H}_C$ to the Coriolis effect, $\mathcal{H}_Z$ to the zonal moon potential, and $\mathcal{H}_{3b}$ to the third-body attraction.

The preceding terms are

$$\mathcal{H}_K=\frac{1}{2}\boldsymbol{X}\cdot\boldsymbol{X}-\frac{\mu}{r}=\frac{1}{2}\left(R^2+\frac{\Theta^2}{r^2}\right)-\frac{\mu}{r}$$
$$\mathcal{H}_C=-\boldsymbol{\omega}\cdot(\boldsymbol{x}\times\boldsymbol{X})=-\omega N$$
$$\mathcal{H}_Z=\sum_{n\geq 2}\frac{\mu}{r}\left(\frac{\alpha}{r}\right)^n J_nP_n(\sin i\sin(f+g))$$
$$\mathcal{H}_{3b}=\frac{\omega^2r^2}{2}(1-3[\cos h\cos(f+g)-\sin h\sin(f+g)\cos i]^2)$$

where $(r,\theta,\nu,R,\Theta,N)$ are the polar-nodal canonical variables, i the inclination, f the true anomaly, g the argument of the pericenter, and h the nodal angle.

The preceding expression for the Hamiltonian is general; however, depending on the type of mission, some simplifications may be introduced. As proved in [18] the third-body attraction is almost negligible for orbits whose altitude is below 100 km, thus, for low orbits we take the Hamiltonian

$$\mathcal{H}_l=\mathcal{H}_0+\epsilon\mathcal{H}_1 \tag{4}$$

with $\mathcal{H}_0=\mathcal{H}_K$, $\epsilon\mathcal{H}_1=\mathcal{H}_Z$, and the small parameter $\epsilon=J_2$. Note that we drop the term $\mathcal{H}_C$ because the nodal angle ν does not appear in the Hamiltonian, and, hence, its conjugate momentum N is a first integral.

For altitudes higher than 100 km it is necessary to consider the third-body perturbation effect $\mathcal{H}_{3b}$, as well as the Coriolis term $\mathcal{H}_C$ because the nodal angle explicitly appears in $\mathcal{H}_{3b}$. Now, a new "Hamiltonian scaling" is in order. Let n be the mean motion of the orbiter, assuming its orbit Keplerian. We then introduce the small parameter $\epsilon=\omega/n$, and, thus, after rearranging the terms, the Hamiltonian for moderate altitudes (that is, $a<3\alpha$) may be written as

$$\mathcal{H}_m=\mathcal{H}_0+\epsilon\mathcal{H}_1+\frac{\epsilon^2}{2}\mathcal{H}_2 \tag{5}$$

with $\mathcal{H}_0=\mathcal{H}_K$, $\epsilon\mathcal{H}_1=\mathcal{H}_C$, and $\epsilon^2\mathcal{H}_2/2=\mathcal{H}_{3b}+\mathcal{H}_Z$. It was proved in [3,19] that the main contributors to the global pictures of frozen orbits about the moon are the J_2 and J_7 harmonic coefficients; this is the reason why in our study we only consider these two harmonics in the zonal part $\mathcal{H}_Z$.

III. Lie Transforms for Hamiltonian Systems

Analytical theories have been widely used to obtain approximated solutions for the problem of the artificial satellite theory since the pioneering works of Brouwer and Clemence [20,21], Kozai [22], Garfinkel [23]. Many other outstanding researchers have devoted a large effort to provide different solutions; new general perturbations theories were invented [24,25] and even symbolic algebraic processors were built with the aim of computing automatically those theories (e.g., Deprit [26] and Abad et al. [27] and references therein). It must be noted that analytical theories can be used to obtain a deeper qualitative insight into the problem by determining the phase flow evolution, equilibria, bifurcations, etc. [11,12].

Let us give here a short description of the general algorithms of the Lie transforms and the one used in this paper; for more details the reader is referred to the original work of Deprit [25], or to the tutorial [28].

A Lie transform of generator W is a near-identity canonical transformation φ: $(\boldsymbol{y},\boldsymbol{Y};\epsilon)\to(\boldsymbol{x},\boldsymbol{X})$, such that $\boldsymbol{x}(\boldsymbol{y},\boldsymbol{Y};\epsilon)$ and $\boldsymbol{X}(\boldsymbol{y},\boldsymbol{Y};\epsilon)$ verify

$$\frac{\mathrm{d}\boldsymbol{x}}{\mathrm{d}\epsilon}=\frac{\partial W}{\partial\boldsymbol{X}},\qquad\frac{\mathrm{d}\boldsymbol{X}}{\mathrm{d}\epsilon}=-\frac{\partial W}{\partial\boldsymbol{x}}$$

with initial conditions $\boldsymbol{x}(\boldsymbol{y},\boldsymbol{Y};0)=\boldsymbol{y}$ and $\boldsymbol{X}(\boldsymbol{y},\boldsymbol{Y};0)=\boldsymbol{X}$.

Let us now consider a Hamiltonian that is a power series of the small parameter ϵ

$$\mathcal{H}(\boldsymbol{x},\boldsymbol{X};\epsilon)=\sum_{n\geq 0}\frac{\epsilon^n}{n!}\mathcal{H}_n(\boldsymbol{x},\boldsymbol{X})=\sum_{n\geq 0}\frac{\epsilon^n}{n!}\mathcal{H}_{n,0}(\boldsymbol{x},\boldsymbol{X}) \tag{6}$$

and a Lie transform whose generating function is the series

$$W(\boldsymbol{x},\boldsymbol{X};\epsilon)=\sum_{n\geq 0}\frac{\epsilon^n}{n!}W_{n+1}(\boldsymbol{x},\boldsymbol{X})$$

we may ask ourselves how this Hamiltonian is affected by the Lie transform.

In his famous paper, Deprit [25] gave a method to build up the transformation term by term in a recursive way by means of the so-called *Lie triangle*

$$\mathcal{H}_{i,j}=\mathcal{H}_{i+1,j-1}+\sum_{0\leq k\leq i}\binom{i}{j}\{\mathcal{H}_{k,j-1},W_{i+1-k}\} \tag{7}$$

for $i\geq 0$ and $j\geq 1$, and where $\{-;-\}$ stands for the Poisson bracket. This procedure makes the task of automatizing the method simple.

The new Hamiltonian, denoted by $\mathcal{K}$, is

$$\mathcal{K}(\boldsymbol{y},\boldsymbol{Y};\epsilon)=\sum_{n\geq 0}\frac{\epsilon^n}{n!}\mathcal{K}_n(\boldsymbol{y},\boldsymbol{Y})=\sum_{n\geq 0}\frac{\epsilon^n}{n!}\mathcal{H}_{0,n}(\boldsymbol{y},\boldsymbol{Y})$$

The generating function is normally not known, and it must be determined term by term by means of Eq. (7) in order for the new Hamiltonian to satisfy some predetermined conditions or requirements. The generating function is thus obtained by solving the PDE (partial differential equation) in Eq. (7), which may be put in the form of the so-called *homologic equation*

$$\mathcal{L}_0(W_n)+\mathcal{K}_n=\tilde{\mathcal{H}}_{0,n} \tag{8}$$

where $\tilde{\mathcal{H}}_{0,n}$ collects all the terms known from the previous order and $\mathcal{L}_0(-)$ is the Lie derivative operator (i.e., $\mathcal{L}_0(-)=\{-,\mathcal{H}_0\}$).

Once the generating function W is obtained, the transformation is given by

$$\boldsymbol{x} = \boldsymbol{y} + \sum_{n\geq 1} \frac{\epsilon^n}{n!} \mathcal{L}_W^n(\boldsymbol{y}), \qquad \boldsymbol{X} = \boldsymbol{Y} + \sum_{n\geq 1} \frac{\epsilon^n}{n!} \mathcal{L}_W^n(\boldsymbol{Y}) \tag{9}$$

whereas the inverse transformation is

$$\boldsymbol{y} = \boldsymbol{x} + \sum_{n\geq 1} \frac{\epsilon^n}{n!} \mathcal{L}_{(-W)}^n(\boldsymbol{x}), \qquad \boldsymbol{Y} = \boldsymbol{X} + \sum_{n\geq 1} \frac{\epsilon^n}{n!} \mathcal{L}_{(-W)}^n(\boldsymbol{X}) \tag{10}$$

It is necessary to determine the properties that the new Hamiltonian must satisfy. The main goal of analytical theories is to reduce the original Hamiltonian by means of Lie transformations and in such a way that the new Hamiltonian is simple enough, and ideally completely integrable, that is to say, that the new Hamiltonian does not contain any angle, although this challenge is not always accomplished.

From Eq. (8), the term $\mathcal{H}_0$ plays an outstanding role, because it is necessary to compute the Lie derivative $\mathcal{L}_0$ with respect to it, thus, the simpler the expression of $\mathcal{H}_0$, the easier is to compute the Lie derivative.

In the Delaunay map (ℓ, g, h, L, G, H), the Keplerian Hamiltonian reads

$$\mathcal{H}_0 = -\frac{\mu^2}{2L^2} \tag{11}$$

The Lie derivative $\mathcal{L}_0$: $F \mapsto \{F; \mathcal{H}_0\}$ in the vector field generated by $\mathcal{H}_0$ is very simple indeed; it is just the differential operator

$$\mathcal{L}_0 = n\frac{\partial}{\partial \ell} \quad \text{with} \quad n = \frac{\mu^2}{L^3} \tag{12}$$

and the PDE to be solved, at each order n of the transformation, according to Eq. (8) is

$$n\frac{\partial W_n}{\partial \ell} + \mathcal{K}_n = \tilde{H}_{0,n}$$

It still remains to determine what we want to obtain after a Lie transformation. Ideally, we would like to have a new Hamiltonian independent of some variables, which is known as a *normalization*, but this goal is not always possible and usually it requires expansions in terms of the eccentricity (valid only for almost-circular orbits) or a big amount of symbolic computation. Deprit and Miller [29,30] introduced other transformations dubbed *simplifications* that do not eliminate the variables, but convert the original Hamiltonian into another one, simpler than the original, and to which normalization techniques may be applied. By so doing, the amount of computation is reduced drastically. However, in our case, we do not need to use these types of transformations.

Essentially, a *Delaunay normalization* [31] consists of removing all the coordinates from the Hamiltonian by means of Lie transforms. The kernel of the Lie derivative along the Hamiltonian flow of the pure Kepler problem is

$$\ker(\mathcal{L}_0) = \{F(\ell, g, h, L, G, H) | \mathcal{L}_0(F) = 0\}$$

Consequently, as the Delaunay action L is an integral of $\mathcal{H}_0$, it generates an infinitesimal contact transformation [31]. The purpose of this local map is to replace the perturbation $\mathcal{R}$ by $\mathcal{R}'$ such that $\mathcal{R}' \in \ker(\mathcal{L}_0)$. Then it appears that the symmetrization induced by the new Delaunay action L' is obtained by eliminating ℓ' from the transformed Hamiltonian $\mathcal{H}'$. As a side effect, the normalization of Eq. (3) allows for the reduction of the number of degrees of freedom by one unit $\mathcal{H} \equiv \mathcal{H}(g', h', G', H')$.

IV. Analytical Integration

We are dealing with two Hamiltonians, $\mathcal{H}_l$ and $\mathcal{H}_m$, depending on whether the satellite is at low or moderate altitude. Although they are different from each other, both Hamiltonians share some common parts. Indeed, in both cases, the zero-order Hamiltonian is the Kepler problem, $\mathcal{H}_0 = \mathcal{H}_K$. Thus, because the Lie derivative is given in Eq. (12), to carry out the Delaunay normalization, the new Hamiltonian chosen is the averaged Hamiltonian over the mean anomaly ℓ

$$\mathcal{K}_n = \frac{1}{2\pi}\int_0^{2\pi} \tilde{\mathcal{H}}_n \mathrm{d}\ell \tag{13}$$

hence the homologic equation gives

$$W_n = \frac{1}{n}\int (\tilde{\mathcal{H}}_n - \mathcal{K}_n)\mathrm{d}\ell \tag{14}$$

The Delaunay normalization removes 1 degree of freedom because it makes the angle ℓ cyclic; hence, its conjugate action L is an integral. After the Delaunay normalization the Hamiltonian corresponding to low orbit $\mathcal{K}_l$ has only 1 degree of freedom; it contains only one angle, the pericenter g; we only need a first-order transformation and we stop the process of applying more Lie transforms to the Hamiltonian $\mathcal{K}_l$. On the contrary, for moderate altitudes, the normalized Hamiltonian $\mathcal{K}_m$ has 2 degrees of freedom because it contains the angles g and h. In this case, we need a second-order transformation, and to the new Hamiltonian, we have to apply another normalization to eliminate the node h.

In the case of low-altitude orbits in Eq. (4), the first-order normalized Hamiltonian is

$$\begin{aligned}
\mathcal{K}_l = &-\frac{\mu^2}{2L^2} + \left(-\frac{J_2\alpha^2\mu^4}{2L^6\eta^3} + \frac{3J_2 s^2\alpha^2\mu^4}{4L^6\eta^3}\right) \\
&+ \left(\frac{225225eJ_7s^7\alpha^7\mu^9}{8192L^{16}\eta^9} - \frac{51975eJ_7s^5\alpha^7\mu^9}{1024L^{16}\eta^9} + \frac{14175eJ_7s^3\alpha^7\mu^9}{512L^{16}\eta^9}\right. \\
&- \frac{525eJ_7s\alpha^7\mu^9}{128L^{16}\eta^9} - \frac{675675eJ_7s^7\alpha^7\mu^9}{4096L^{16}\eta^{11}} + \frac{155925eJ_7s^5\alpha^7\mu^9}{512L^{16}\eta^{11}} \\
&- \frac{42525eJ_7s^3\alpha^7\mu^9}{256L^{16}\eta^{11}} + \frac{1575eJ_7s\alpha^7\mu^9}{64L^{16}\eta^{11}} + \frac{1486485eJ_7s^7\alpha^7\mu^9}{8192L^{16}\eta^{13}} \\
&- \frac{343035eJ_7s^5\alpha^7\mu^9}{1024L^{16}\eta^{13}} + \frac{93555eJ_7s^3\alpha^7\mu^9}{512L^{16}\eta^{13}} \\
&\left.- \frac{3465eJ_7s\alpha^7\mu^9}{128L^{16}\eta^{13}}\right)\sin g + \left(-\frac{135135eJ_7s^7\alpha^7\mu^9}{16384L^{16}\eta^9}\right. \\
&+ \frac{51975eJ_7s^5\alpha^7\mu^9}{4096L^{16}\eta^9} - \frac{4725eJ_7s^3\alpha^7\mu^9}{1024L^{16}\eta^9} + \frac{315315eJ_7s^7\alpha^7\mu^9}{8192L^{16}\eta^{11}} \\
&- \frac{121275eJ_7s^5\alpha^7\mu^9}{2048L^{16}\eta^{11}} + \frac{11025eJ_7s^3\alpha^7\mu^9}{512L^{16}\eta^{11}} - \frac{495495eJ_7s^7\alpha^7\mu^9}{16384L^{16}\eta^{13}} \\
&\left.+ \frac{190575eJ_7s^5\alpha^7\mu^9}{4096L^{16}\eta^{13}} - \frac{17325eJ_7s^3\alpha^7\mu^9}{1024L^{16}\eta^{13}}\right)\sin 3g \\
&+ \left(\frac{9009eJ_7s^7\alpha^7\mu^9}{16384L^{16}\eta^9} - \frac{2079eJ_7s^5\alpha^7\mu^9}{4096L^{16}\eta^9} - \frac{9009eJ_7s^7\alpha^7\mu^9}{8192L^{16}\eta^{11}}\right. \\
&\left.+ \frac{2079eJ_7s^5\alpha^7\mu^9}{2048L^{16}\eta^{11}} + \frac{9009eJ_7s^7\alpha^7\mu^9}{16384L^{16}\eta^{13}} - \frac{2079eJ_7s^5\alpha^7\mu^9}{4096L^{16}\eta^{13}}\right)\sin 5g
\end{aligned} \tag{15}$$

The generating function of the transformation is too long to be reproduced; it is composed of 467 terms. As usual, $c = \cos i$, $s = \sin i$, and $\eta^2 = 1 - e^2$.

With respect to the Hamiltonian for moderate orbits in Eq. (5), it contains second-order terms, hence we have to carry out the normalization over the mean anomaly ℓ up to the second order. The generating function contains 687 terms, and the normalized Hamiltonian is given in the appendix.

As we already said, the momentum L is an integral of the normalized Hamiltonian, thus, we may drop the first term (Kepler problem) and rearrange the terms in such a way that now the zero-order term is the Coriolis part ($\mathcal{H}_0 = -\omega H$), and the rest will be the first order. (For the sake of simplifying the notation we still use $\mathcal{H}_n$ instead of $\mathcal{K}_n$).

For this normalized Hamiltonian, the Lie operator is now

$$\mathcal{L}_0 = \omega \frac{\partial}{\partial h}$$

and, thus, for the new Hamiltonian we simply choose the averaged Hamiltonian over the angle h. From the homology equation, we get

$$\mathcal{K} = \frac{1}{2\pi}\int_0^{2\pi} \mathcal{H}\mathrm{d}h, \qquad W = \frac{1}{\omega}\int (\mathcal{H} - \mathcal{K})\mathrm{d}h \tag{16}$$

The new Hamiltonian is indeed of 1 DOF in the angle g, and there is no need for further Lie transforms, because with 1 DOF we can explore the topology of the system. The generating function now contains 32 summands, and the twice-normalized Hamiltonian is

$$\begin{aligned}
\mathcal{K}_h = &-H\omega + \left(\frac{3J_2 s^2\alpha^2\mu^4}{8L^6\eta^3} - \frac{J_2\alpha^2\mu^4}{4L^6\eta^3} - \frac{5L^4\omega^2}{16\mu^2} + \frac{15L^4 s^2\omega^2}{32\mu^2}\right.\\
&\left. + \frac{3L^4\eta^2\omega^2}{16\mu^2} - \frac{9L^4 s^2\eta^2\omega^2}{32\mu^2}\right) + \left(\frac{225225eJ_7 s^7\alpha^7\mu^9}{16384L^{16}\eta^9}\right.\\
&- \frac{51975eJ_7 s^5\alpha^7\mu^9}{2048L^{16}\eta^9} + \frac{14175eJ_7 s^3\alpha^7\mu^9}{1024L^{16}\eta^9} - \frac{525eJ_7 s\alpha^7\mu^9}{256L^{16}\eta^9}\\
&- \frac{675675eJ_7 s^7\alpha^7\mu^9}{8192L^{16}\eta^{11}} + \frac{155925eJ_7 s^5\alpha^7\mu^9}{1024L^{16}\eta^{11}} - \frac{42525eJ_7 s^3\alpha^7\mu^9}{512L^{16}\eta^{11}}\\
&+ \frac{1575eJ_7 s\alpha^7\mu^9}{128L^{16}\eta^{11}} + \frac{1486485eJ_7 s^7\alpha^7\mu^9}{16384L^{16}\eta^{13}} - \frac{343035eJ_7 s^5\alpha^7\mu^9}{2048L^{16}\eta^{13}}\\
&\left. + \frac{93555eJ_7 s^3\alpha^7\mu^9}{1024L^{16}\eta^{13}} - \frac{3465eJ_7 s\alpha^7\mu^9}{256L^{16}\eta^{13}}\right)\sin g\\
&+ \left(-\frac{135135eJ_7 s^7\alpha^7\mu^9}{32768L^{16}\eta^9} + \frac{51975eJ_7 s^5\alpha^7\mu^9}{8192L^{16}\eta^9} - \frac{4725eJ_7 s^3\alpha^7\mu^9}{2048L^{16}\eta^9}\right.\\
&+ \frac{315315eJ_7 s^7\alpha^7\mu^9}{16384L^{16}\eta^{11}} - \frac{121275eJ_7 s^5\alpha^7\mu^9}{4096L^{16}\eta^{11}} + \frac{11025eJ_7 s^3\alpha^7\mu^9}{1024L^{16}\eta^{11}}\\
&- \frac{495495eJ_7 s^7\alpha^7\mu^9}{32768L^{16}\eta^{13}} + \frac{190575eJ_7 s^5\alpha^7\mu^9}{8192L^{16}\eta^{13}}\\
&\left. - \frac{17325eJ_7 s^3\alpha^7\mu^9}{2048L^{16}\eta^{13}}\right)\sin 3g + \left(\frac{9009eJ_7 s^7\alpha^7\mu^9}{32768L^{16}\eta^9}\right.\\
&- \frac{2079eJ_7 s^5\alpha^7\mu^9}{8192L^{16}\eta^9} - \frac{9009eJ_7 s^7\alpha^7\mu^9}{16384L^{16}\eta^{11}} + \frac{2079eJ_7 s^5\alpha^7\mu^9}{4096L^{16}\eta^{11}}\\
&+ \frac{9009eJ_7 s^7\alpha^7\mu^9}{32768L^{16}\eta^{13}} - \frac{2079eJ_7 s^5\alpha^7\mu^9}{8192L^{16}\eta^{13}}\Big)\sin 5g\\
&+ \left(-\frac{3e^2L^4 s^2\omega^2}{32\mu^2} - \frac{3L^4 s^2\omega^2}{8\mu^2} + \frac{3L^4 s^2\eta^2\omega^2}{8\mu^2}\right)\cos 2g
\end{aligned} \tag{17}$$

In short, after several transformations and a suitable rearranging of terms, the reduced Hamiltonian (for both low and moderate altitude) is of the form

$$\begin{aligned}
\mathcal{K}(-, g, -; L, G, H) = &M_{00} + M_{01}\sin g + M_{03}\sin 3g\\
&+ M_{05}\sin 5g + \delta M_{02}\cos 2g
\end{aligned} \tag{18}$$

where the symbol δ is a parameter that takes the value 0 for low-altitude and 1 for moderate-altitude orbiter, and coefficients M_{ij} may be identified from expressions in Eq. (15) or Eq. (17) and depend on a, e, i, μ, α, ω, J_2, and J_7, but once the fundamental constants are fixed, the coefficients depend only on three orbital elements, namely, a, e, and i.

The equations of motion of the Hamiltonian Eq. (18) are

$$\begin{aligned}
\frac{\mathrm{d}g}{\mathrm{d}t} &= \frac{\partial\mathcal{K}}{\partial G} = m_{00} + m_{01}\sin g + m_{03}\sin 3g\\
&\quad + m_{05}\sin 5g + \delta m_{20}\cos 2g\\
\frac{\mathrm{d}G}{\mathrm{d}t} &= -\frac{\partial\mathcal{K}}{\partial g} = m_{10}\cos g + m_{30}\cos 3g\\
&\quad + m_{50}\cos 5g + \delta m_{02}\sin 2g
\end{aligned} \tag{19}$$

where $m_{i,j}$ are obtained directly from Eq. (18) by partial derivation.

V. Analysis for Low-Altitude Orbits

Frozen orbits correspond to equilibria of the reduced system. In case of low-altitude orbits, the system under consideration is given by making $\delta = 0$ in Eq. (19). Thus, we have to make the right-hand part of these equations equal zero and solve the corresponding system

$$\begin{aligned}
m_{00} + m_{01}\sin g + m_{03}\sin 3g + m_{05}\sin 5g = 0\\
m_{10}\cos g + m_{30}\cos 3g + m_{50}\cos 5g = 0
\end{aligned} \tag{20}$$

To solve this system, we consider two separate cases, namely when $\cos g = 0$ and when $\cos g \neq 0$.

A. Case $\cos g = 0$

The second equation holds when $\cos g = 0$, that is, for $g = \pi/2$, $3\pi/2$; thus, by replacing these values into the first equation of Eq. (20), one equation results depending on three variables, i, a, and e that is represented as a 3-D surface in Fig. 1. Points on this surface correspond to equilibria of the system in Eq. (20), that is, to frozen orbits.

From this figure, curves obtained for constant-a sections are very similar, thus, in order to go into more detail, we fix a semimajor axis $a = \alpha + 100$ km, which indeed corresponds to low orbits. For the chosen value of a, we plot the curve i vs e (see Fig. 2). The horizontal line at $e = 0.054407$ is the limit for impact orbits. The higher the eccentricity is, the shorter is the distance at the pericenter, and, thus, for eccentricities bigger than $e = 0.054407$ the orbiter would impact with the moon surface. Both graphics in Fig. 2 represent the same section, but the one on the right shows fewer values of the eccentricity. The solid line corresponds to $g = \pi/2$, whereas the dashed line is for $g = 3\pi/2$.

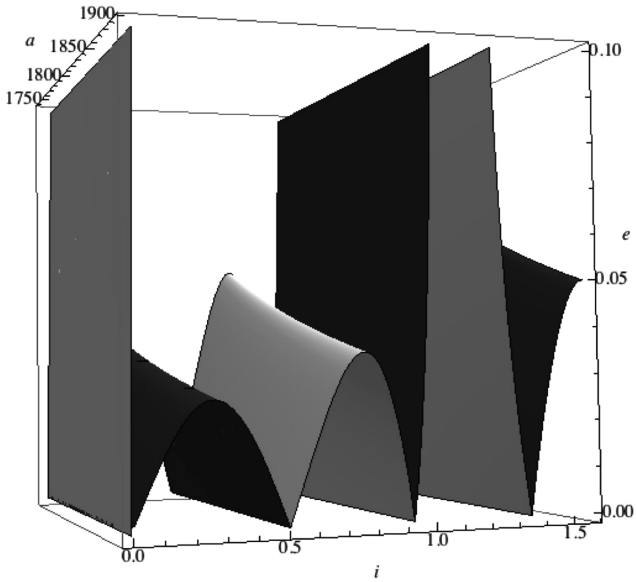

Fig. 1 Surface of frozen orbits for values of i, e, and a and $\cos g = 0$. Black color is the surface when $g = \pi/2$, and the gray is obtained for $g = 3\pi/2$.

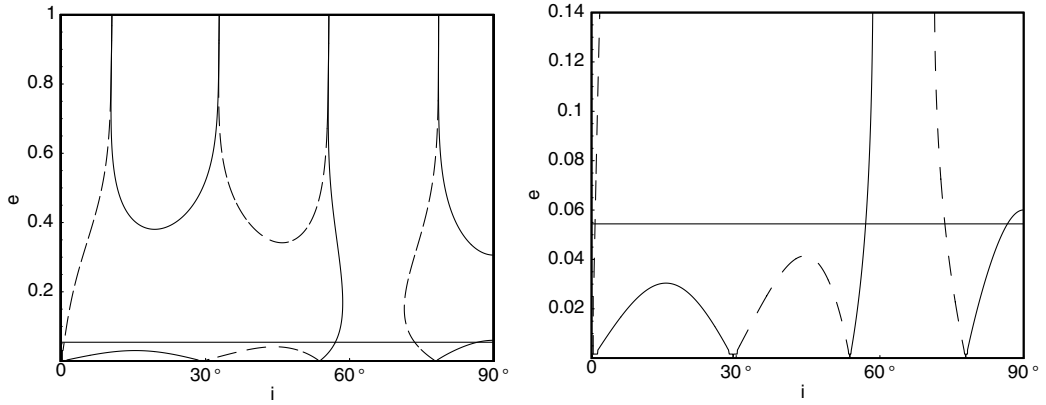

Fig. 2 Frozen orbits for $a = \alpha + 100$ km. The horizontal line $e = 0.054407$ is the limit for impact orbits. The right plot is a part of the left plot, showing fewer values of eccentricity. Dashed lines correspond to $g = \pi/2$ and solid lines to $g = 3\pi/2$.

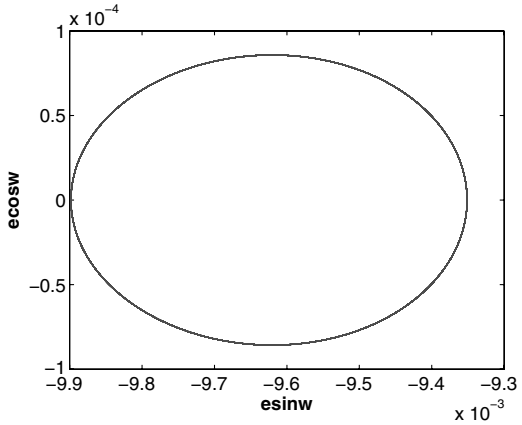

Fig. 3 Periodic orbit for initial conditions $a = 1838$ km, $e = 0.0100186$, and $i = 0.0000527948$ rad, corresponding to the new-found family of almost-equatorial orbits.

When comparing this map of frozen orbits with Fig. 1 given by Elipe and Lara [3], we see that they are almost identical, but in Fig. 2 a new family of almost-equatorial frozen orbits appears, namely the one given by the line very close to the vertical axis, which was not detected in the quoted paper. One might think that this new "family" is an artifact due to truncations of the Lie transforms performed; thus, we check whether or not orbits of this family are periodic and find that they are periodic indeed. Figure 3 includes one such plot.

Note that the frozen orbits detected correspond to the averaged Hamiltonian. As an illustration of how these orbits evolve into the original Hamiltonian, we pick up from the graphics a set of initial conditions of a frozen orbit; then, we apply the initial conditions to an orbit propagator with the initial system and plot the evolution of the orbit in Fig. 4. The graphics on the left correspond to 200 revolutions (almost 20 days), whereas the one on the right corresponds to an integration over 5 years. We clearly see that the frozen character degenerates with time.

However, because the averaged Hamiltonian is obtained through Lie transforms, we have the generating functions of the involved transformations, and by means of the inverse transformation in Eq. (10) we can convert the averaged initial conditions into osculating elements. We then compute the orbit again with the propagator for the same time intervals as in the preceding case, as shown in Fig. 5. For this new set of initial conditions, the orbit still remains almost periodic even after 5 years of integration.

B. Case $\cos g \neq 0$

Let us now consider the case $\cos g \neq 0$. Our first task is to convert the system in Eq. (20) of trigonometric equations into polynomial ones in order to simplify the process of computing the roots of the system. Let us apply $x = \cos g$ and $y = \sin g$ in Eq. (20). Chebyshev polynomials of the *first kind* are defined as $T_n(x) = \cos n(\arccos x)$, that is, $T_n(x) = \cos ng = T_n(\cos g)$, and they satisfy the three terms property

$$T_{n+1}(x) = 2xT_n(x) - T_{n-1}(x), \quad \text{with} \quad T_0(x) = 1, T_1(x) = x$$

Chebyshev polynomials of the *second kind* are defined as $U_n(x) = \sin((n+1)\arccos x)/(\sin(\arccos x))$; in our case $U_n(x) = \sin((n+1)g)/(\sin g)$, and they satisfy the three terms property

$$U_{n+1}(x) = 2xU_n(x) - U_{n-1}(x), \quad \text{with} \quad U_0(x) = 1, U_1(x) = 2x$$

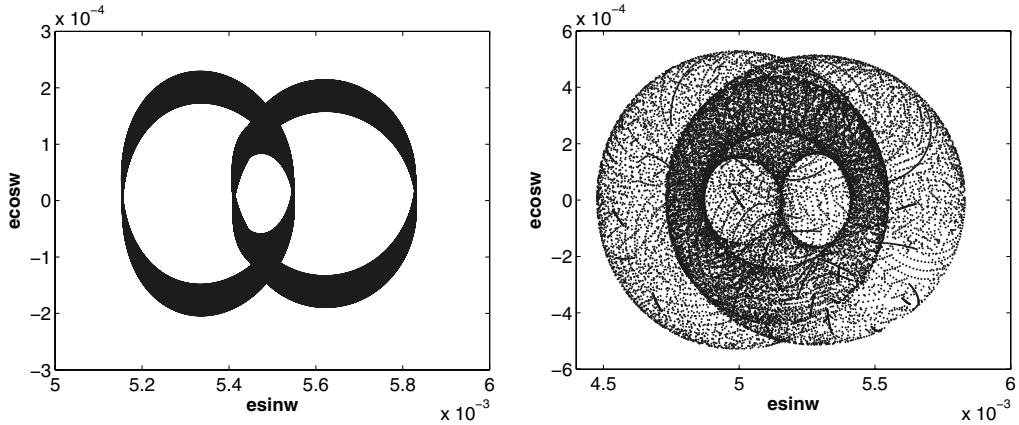

Fig. 4 Orbit evolution ($e \sin \omega$, $e \cos \omega$) of a frozen orbit with averaged initial conditions. Left: Evolution after 20 days of a frozen orbit; right: evolution after 5 years.

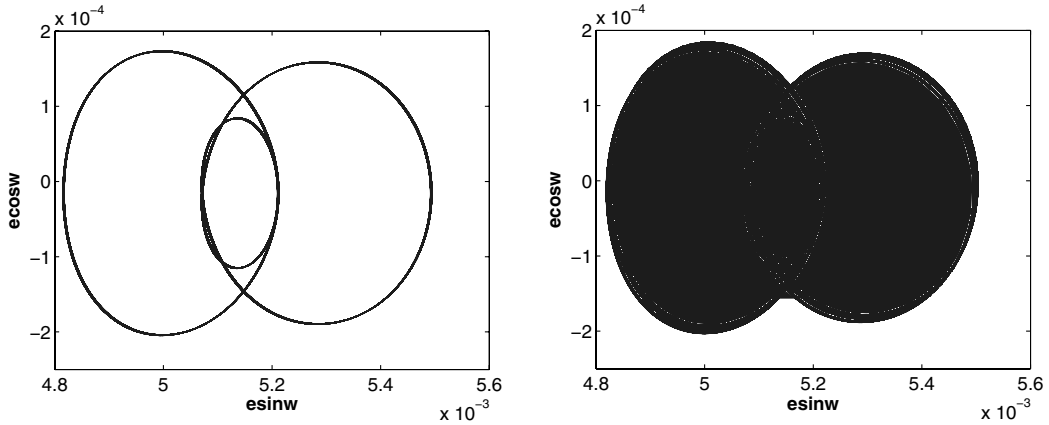

Fig. 5 Orbit evolution ($e\sin\omega$, $e\cos\omega$) of a frozen orbit with osculating initial conditions, obtained by the inverse of the Lie transforms. Left: Evolution after 20 days of a frozen orbit; right: evolution after 5 years.

With these definitions, the system in Eq. (20) is easily elaborated as

$$\begin{aligned} m_{00} + k_{10}y + k_{12}yx^2 + k_{14}yx^4 = 0 \\ x\left(k_{00} + k_{02}x^2 + k_{04}x^4\right) = 0 \end{aligned} \tag{21}$$

where coefficients k_{ij} are functions of a, e, and i. Excluding the case $x = \cos g = 0$, already analyzed in the previous subsection, the second equation is fulfilled when $k_{00} + k_{02}x^2 + k_{04}x^4 = 0$, a quadratic equation in $x^2 = \beta$. From the possible solutions, only those in the interval $0 < \beta = x^2 < 1$ are of interest, because $|x = \cos g| \leq 1$. By replacing the valid solutions in the first equation of the preceding system, the value $y = \sin g$ is obtained, and, thus, the angle g of the frozen orbit.

A numerical search of the roots has been made for the particular cases of the semimajor axis, and the result for $a = \alpha + 100$ km is represented in Fig. 6. Similar results are obtained for other values of a.

The restriction $0 < \beta_j(a, e, i) < 1$ $(j = 1, 2)$ compels the possible values of e and i to lie inside the "triangular" bands that seem to spring out from a certain inclinations (Fig. 6). But the possible solutions within these strips must also satisfy the first equation of the system in Eq. (21). From all possible solutions only values of the solid line crossing the first band (the one emanating from $i = 30$ deg) correspond to frozen orbits. However, these orbits are far beyond the impact orbits, and consequently we conclude that there are no frozen orbits except those found for $\cos g = 0$.

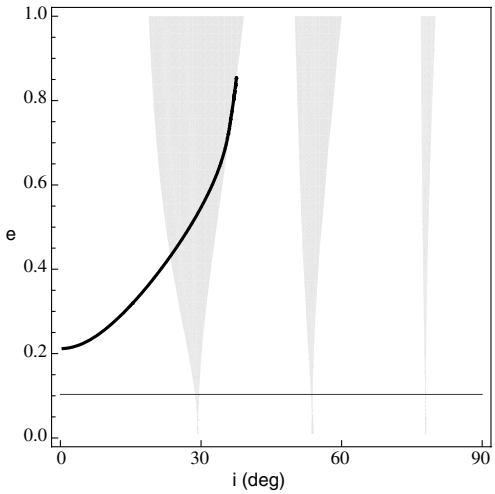

Fig. 6 Frozen orbits (i, e) for $\cos g \neq 0$. Only the line crossing the first strip emanating from $i \approx 30$ deg corresponds to frozen orbits. Note that those are impact orbits and, hence, useless.

VI. Analysis for Moderate-Altitude Orbits

For moderate-altitude orbits, we must make $\delta = 1$ in the equations of motion in Eq. (19). The system is converted into

$$\begin{aligned} m_{00} + m_{01}\sin g + m_{03}\sin 3g + m_{05}\sin 5g + m_{20}\cos 2g = 0 \\ m_{10}\cos g + m_{30}\cos 3g + m_{50}\cos 5g + m_{02}\sin 2g = 0 \end{aligned} \tag{22}$$

The second equation is fulfilled for either $g = \pi/2$ or $g = 3\pi/2$, and therefore, for these two values we can proceed as in we did for low orbits in the previous section. The different families of frozen orbits for several values of the semimajor axis

Table 1 Initial conditions for frozen orbits. The first row of each pair corresponds to averaged initial conditions for the $J_2 + J_7$ problem. The second row corresponds to the actual initial conditions of the original problem ($J_2 + \ldots + J_9$) obtained from the previous problem after a numerical correction procedure

$\tilde{x}$	$\tilde{y}$	$\tilde{z}$	$\dot{\tilde{x}}$	$\dot{\tilde{y}}$	$\dot{\tilde{z}}$
x	y	z	$\dot{x}$	$\dot{y}$	$\dot{z}$
−610.34124124	1619.76000650	434.01271243	−1.58588106	−0.53982315	−0.14464495
−599.66436522	1591.42507580	428.14175270	−1.61476199	−0.54772361	−0.12808443
−157.84486971	1635.13819594	762.47683983	−1.65122224	−0.12902326	−0.06016448
−159.19844058	1649.16003545	772.46673519	−1.63536102	−0.14679905	−0.02295428
−63.14070550	1037.09127710	1481.11956091	−1.65803875	−0.03269739	−0.04669670
−61.08140016	1003.26701777	1431.24121150	−1.71337678	−0.04301879	−0.04004489
607.06597246	−1277.68556609	−1072.10548727	1.59516425	0.42819541	0.35929861
597.80117495	−1258.18604118	−1060.97165345	1.61853377	0.43767831	0.34822062
153.49663258	−1240.60084373	−1240.60084373	1.69702042	0.10074247	0.10074247
153.89202203	−1243.79648699	−1244.07061534	1.69262573	0.10076326	0.10065479
62.32432834	−1147.20570654	−1367.18652221	1.67931055	0.03665314	0.04368151
63.13665947	−1162.15830908	−1385.78703895	1.65760746	0.03796115	0.04255252

a are given in Fig. A of Appendix A. The horizontal lines represent the eccentricity limit for impact orbits; for e beyond this limit, the orbits are useless because they impact with the moon's surface. As the semimajor axis increases, the third-body influence increases. The effect of this influence is a certain flattening of the curves representing the families, that is, comparing graphics in Fig. A1 with the ones in Fig. 2, we see that the behavior is similar, although the eccentricity of the periodic orbits decreases in Fig. A1. In addition, the gap between $i \in (40, 60\,\text{deg})$ is reduced, and the two lines tend to join one another for large values of the semimajor axis a. Thus, when the third-body action is taken into account, most of the frozen orbits are circular, and the only eccentric orbits are either almost circular or near a certain *critical inclination* $\in (40, 60\,\text{deg})$.

For values of the pericenter $g \neq \pi/2$ and $g \neq 3\pi/2$, we could proceed as in the previous section. However, we leave this case for now, because the experience for low orbits suggests that the possible frozen orbits will be of impact.

VII. Frozen Orbits in the Original Problem

In the previous sections we have seen that Lie transforms provide a good approach to detecting frozen orbits. However, the model used is rather simple because, as a matter of fact, only the J_2 and J_7 harmonics from the zonal potential are considered. One can easily guess that frozen orbits for this model are no longer frozen when more complex force functions are considered. However, the averaged initial conditions from the simplified model may be used as the beginnings of numerical correction procedures in order to have frozen orbits for the more complete model.

As a corrector procedure we will use that given by Deprit and Henrard [16], which has already been used in computing frozen orbits for the zonal problem [3,9]. As usual, this corrector method has to be initialized with an almost-periodic orbit, such that after several iterations a periodic orbit is obtained. To begin, we take a periodic orbit from the averaged $J_2 + J_7$ Hamiltonian; this orbit will be almost periodic in the $J_2 + \cdots + J_9$ potential. Hence we are able to apply the corrector procedure, and we will obtain an exact periodic orbit in the $J_2 + \cdots + J_9$ potential. The computations have been obtained with the program coded in MATLAB by E. Tresaco.

As an illustration, we give in Table 1 (first rows) the initial conditions of six almost-periodic orbits (obtained from the averaged Hamiltonian of the $J_2 + J_7$ potential), and in the second rows the initial conditions of the exact periodic orbits of the $J_2 + \cdots + J_9$ potential, obtained with the corrector procedure. Those orbits are plotted in Figs. A2 and A3. In both Figures, the left column contains almost-periodic orbits of the total problem, whereas the right column has exact periodic orbits of the total problem; their initial conditions have been obtained by the corrector method.

VIII. Conclusions

Analytical theories based on Lie–Deprit series are used to compute frozen orbits for an orbiter around the moon. Both low and moderate orbits are analyzed. Even for low-order normalization, the normalized Hamiltonian gives a map with the families of frozen orbits. A new family of almost-equatorial orbits is detected. The inverse transformation allows for a refining of the initial conditions of the frozen orbit; these initial conditions may be used as a starter in a correction scheme for having more accurate frozen orbits when more terms in the force function are included.

Appendix

First-order Hamiltonian for moderate-altitude orbits

$$
\begin{aligned}
\mathcal{H}_h = {} & -\frac{\mu^2}{2L^2} - H\omega + \left(-\frac{J_2\alpha^2\mu^4}{4L^6\eta^3} + \frac{3J_2s^2\alpha^2\mu^4}{8L^6\eta^3} - \frac{5L^4\omega^2}{16\mu^2} + \frac{15L^4s^2\omega^2}{32\mu^2} + \frac{3L^4\eta^2\omega^2}{16\mu^2} - \frac{9L^4s^2\eta^2\omega^2}{32\mu^2}\right) \\
& + \left(\frac{225225eJ_7s^7\alpha^7\mu^9}{16384L^{16}\eta^9} - \frac{51975eJ_7s^5\alpha^7\mu^9}{2048L^{16}\eta^9}\right. \\
& + \frac{14175eJ_7s^3\alpha^7\mu^9}{1024L^{16}\eta^9} - \frac{525eJ_7s\alpha^7\mu^9}{256L^{16}\eta^9} - \frac{675675eJ_7s^7\alpha^7\mu^9}{8192L^{16}\eta^{11}} + \frac{155925eJ_7s^5\alpha^7\mu^9}{1024L^{16}\eta^{11}} - \frac{42525eJ_7s^3\alpha^7\mu^9}{512L^{16}\eta^{11}} \\
& \left. + \frac{1575eJ_7s\alpha^7\mu^9}{128L^{16}\eta^{11}} > + \frac{1486485eJ_7s^7\alpha^7\mu^9}{16384L^{16}\eta^{13}} - \frac{343035eJ_7s^5\alpha^7\mu^9}{2048L^{16}\eta^{13}} + \frac{93555eJ_7s^3\alpha^7\mu^9}{1024L^{16}\eta^{13}} - \frac{3465eJ_7s\alpha^7\mu^9}{256L^{16}\eta^{13}}\right)\sin g \\
& + \left(-\frac{135135eJ_7s^7\alpha^7\mu^9}{32768L^{16}\eta^9} + \frac{51975eJ_7s^5\alpha^7\mu^9}{8192L^{16}\eta^9} - \frac{4725eJ_7s^3\alpha^7\mu^9}{2048L^{16}\eta^9} + \frac{315315eJ_7s^7\alpha^7\mu^9}{16384L^{16}\eta^{11}} - \frac{121275eJ_7s^5\alpha^7\mu^9}{4096L^{16}\eta^{11}} + \frac{11025eJ_7s^3\alpha^7\mu^9}{1024L^{16}\eta^{11}}\right. \\
& \left. - \frac{495495eJ_7s^7\alpha^7\mu^9}{32768L^{16}\eta^{13}} + \frac{190575eJ_7s^5\alpha^7\mu^9}{8192L^{16}\eta^{13}} - \frac{17325eJ_7s^3\alpha^7\mu^9}{2048L^{16}\eta^{13}}\right)\sin 3g + \left(\frac{9009eJ_7s^7\alpha^7\mu^9}{32768L^{16}\eta^9} - \frac{2079eJ_7s^5\alpha^7\mu^9}{8192L^{16}\eta^9} - \frac{9009eJ_7s^7\alpha^7\mu^9}{16384L^{16}\eta^{11}}\right. \\
& \left. + \frac{2079eJ_7s^5\alpha^7\mu^9}{4096L^{16}\eta^{11}} + \frac{9009eJ_7s^7\alpha^7\mu^9}{32768L^{16}\eta^{13}} - \frac{2079eJ_7s^5\alpha^7\mu^9}{8192L^{16}\eta^{13}}\right)\sin 5g + \left(-\frac{3L^4s^2\eta^4\omega^2}{8e^2\mu^2} - \frac{3L^4s^2\omega^2}{8e^2\mu^2} - \frac{3L^4s^2\omega^2}{32\mu^2} + \frac{3L^4s^2\eta^2\omega^2}{4e^2\mu^2}\right. \\
& \left. + \frac{3L^4s^2\eta^2\omega^2}{32\mu^2}\right)\cos 2g + \left(-\frac{15L^4s^2\omega^2}{32\mu^2} + \frac{9L^4s^2\eta^2\omega^2}{32\mu^2}\right)\cos 2h + \left(\frac{3cL^4\omega^2}{32\mu^2} + \frac{3cL^4\omega^2}{8e^2\mu^2} - \frac{3L^4\omega^2}{8e^2\mu^2} - \frac{3L^4\omega^2}{32\mu^2} + \frac{3cL^4\eta^4\omega^2}{8e^2\mu^2} - \frac{3L^4\eta^4\omega^2}{8e^2\mu^2}\right. \\
& \left. + \frac{3L^4s^2\eta^4\omega^2}{16e^2\mu^2} + \frac{3L^4s^2\omega^2}{16e^2\mu^2} + \frac{3L^4s^2\omega^2}{64\mu^2} - \frac{3cL^4\eta^2\omega^2}{32\mu^2} - \frac{3cL^4\eta^2\omega^2}{4e^2\mu^2} + \frac{3L^4\eta^2\omega^2}{4e^2\mu^2} + \frac{3L^4\eta^2\omega^2}{32\mu^2} - \frac{3L^4s^2\eta^2\omega^2}{8e^2\mu^2} - \frac{3L^4s^2\eta^2\omega^2}{64\mu^2}\right)\cos(2g-2h) \\
& + \left(-\frac{3cL^4\omega^2}{32\mu^2} - \frac{3cL^4\omega^2}{8e^2\mu^2} - \frac{3L^4\omega^2}{8e^2\mu^2} - \frac{3L^4\omega^2}{32\mu^2} - \frac{3cL^4\eta^4\omega^2}{8e^2\mu^2} - \frac{3L^4\eta^4\omega^2}{8e^2\mu^2} + \frac{3L^4s^2\eta^4\omega^2}{16e^2\mu^2} + \frac{3L^4s^2\omega^2}{16e^2\mu^2} + \frac{3L^4s^2\omega^2}{64\mu^2} + \frac{3cL^4\eta^2\omega^2}{32\mu^2}\right. \\
& \left. + \frac{3cL^4\eta^2\omega^2}{4e^2\mu^2} + \frac{3L^4\eta^2\omega^2}{4e^2\mu^2} + \frac{3L^4\eta^2\omega^2}{32\mu^2} - \frac{3L^4s^2\eta^2\omega^2}{8e^2\mu^2} - \frac{3L^4s^2\eta^2\omega^2}{64\mu^2}\right)\cos(2g+2h)
\end{aligned}
$$

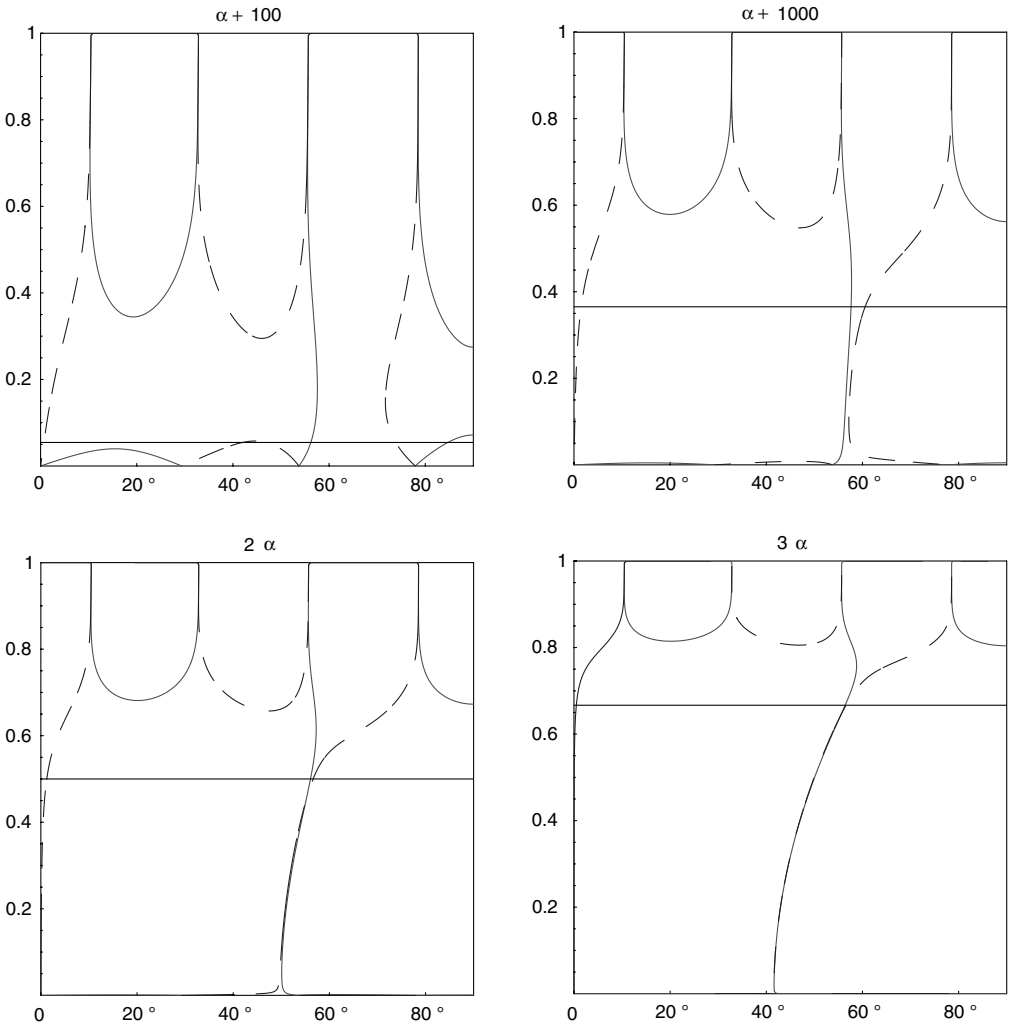

Fig. A1 Families of frozen orbits corresponding to moderate altitudes and several values of the semimajor axis: $a = \alpha + 100$ km, $a = \alpha + 1000$ km, $a = 2\alpha$, and $a = 3\alpha$. The horizontal lines represent the eccentricity limit for impact orbits.

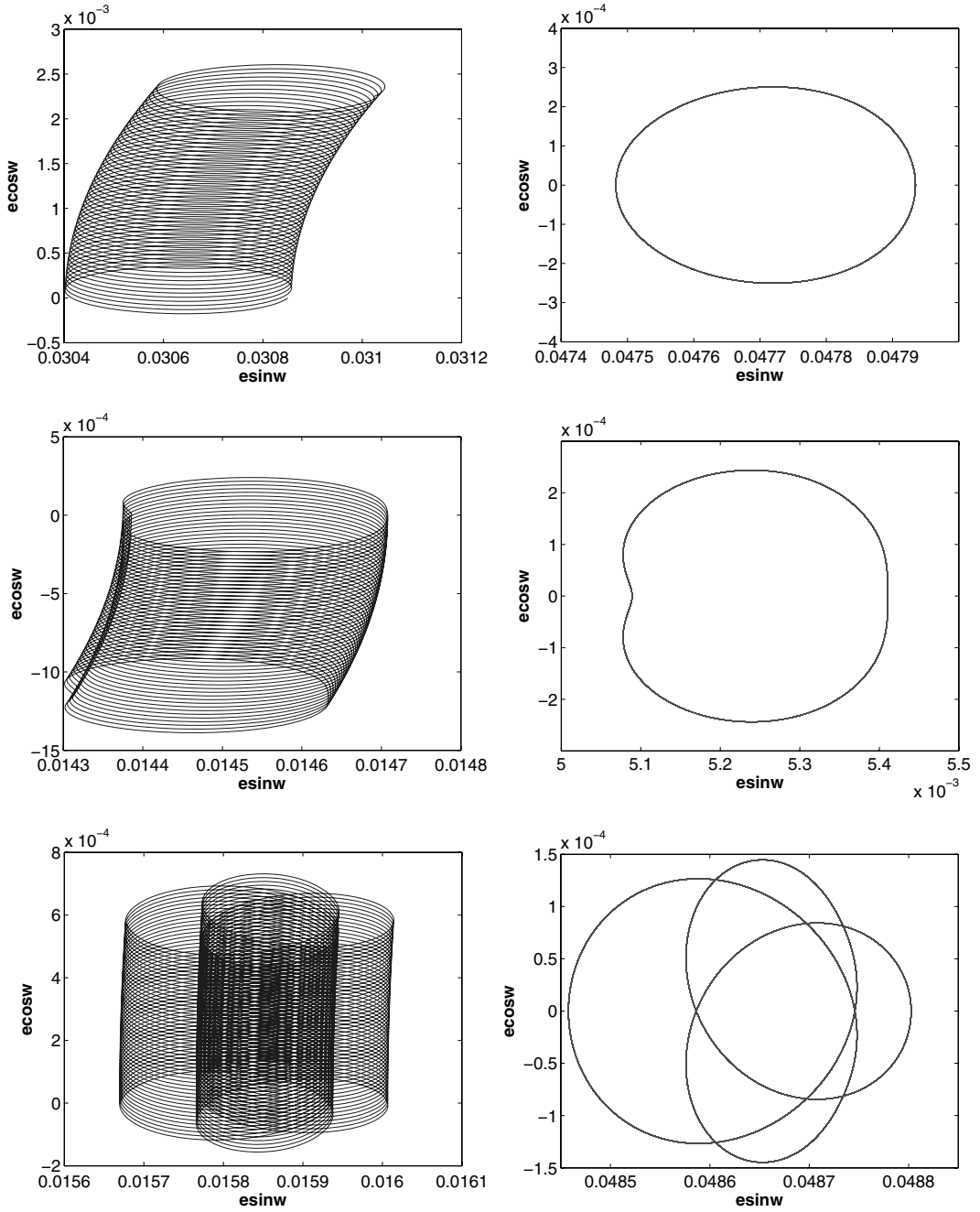

Fig. A2 Orbits for the first three pairs of initial conditions of Table 1. Left column: orbits in the total problem with averaged initial conditions (these orbits are not periodic). Note that these plots are 2-D. Right column: orbits in the total problem with corrected initial conditions (these orbits are periodic).

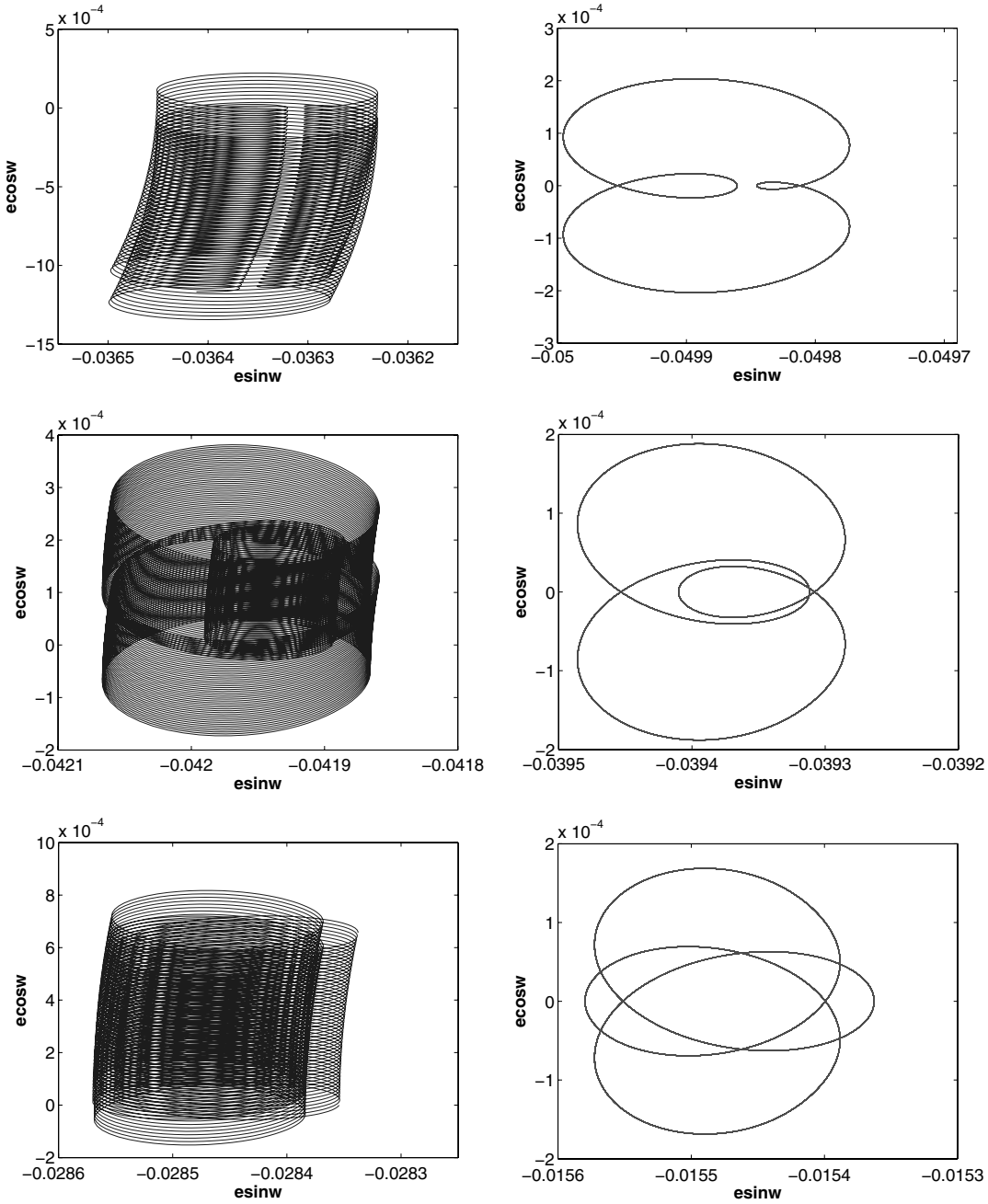

Fig. A3 Orbits for the last three pairs of initial conditions of Table 1. Left column: orbits in the total problem with averaged initial conditions (these orbits are not periodic). Note also that these plots are 2-D. Right column: orbits in the total problem with corrected initial conditions (these orbits are periodic).

Acknowledgments

This research has been supported by the Spanish Ministry of Science and Technology (Projects no. ESP2005-07107 and no. MTM2006-06961). Discussions with Martín Lara and Juan F. San-Juan at the first steps of this work were very fruitful. Authors are grateful to Juan San-Juan for allowing them to use his software MathATESAT for computing Lie transformations.

References

[1] Park, S. Y., and Junkins, J. L., "Orbital Mission Analysis for a Lunar Mapping Satellite," *Journal of the Astronautical Sciences*, Vol. 43, No. 2, 1995, pp. 207–217.

[2] Scheeres, D. J., Williams, B. G., and Miller, J. K., "Evaluation of the Dynamic Environment of an Asteroid: Applications to 433 Eros," *Journal of Guidance, Control and Dynamics*, Vol. 23, No. 3, 2000, pp. 466–475. doi:10.2514/2.4552

[3] Elipe, A., and Lara, M., "Frozen Orbits About the Moon," *Journal of Guidance, Control and Dynamics*, Vol. 26, No. 2, 2003, pp. 238–243. doi:10.2514/2.5064

[4] Elipe, A., and Lara, M., "A Simple Model for the Chaotic Motion Around (433) Eros," *Journal of the Astronautical Sciences*, Vol. 51, No. 4, 2003, pp. 391–404.

[5] San-Juan, J. F., Abad, A., Lara, M., and Scheeres, D. J., "First-Order Analytical Solution for Spacecraft Motion About (433) Eros," *Journal of Guidance, Control and Dynamics*, Vol. 27, No. 2, 2004, pp. 290–293. doi:10.2514/1.9171

[6] Lara, M., and Russell, R., "Computation of a Science Orbit About Europa," *Journal of Guidance, Control and Dynamics*, Vol. 30, No. 1, 2007, pp. 259–263. doi:10.2514/1.22493

[7] Elipe, A., Arribas, M., and Kalvouridis, T., "Periodic Solutions and their Parametric Evolution in the Planar Case of the $(n+1)$ Ring Problem with Oblateness," *Journal of Guidance, Control and Dynamics*, Vol. 30, No. 6, 2007, pp. 1640–1648.

[8] Scheeres, D. J., "Satellite Dynamics About Asteroids: Computing Poincaré Maps for the General Case," *Hamiltonian Systems with Three or More Degrees of Freedom*, edited by C. Simó, NATO ASI Series C, Kluwer Academic, Norwell, MA, Vol. 533, 1999, pp. 554–557.

[9] Lara, M., Deprit, A., and Elipe, A., "Numerical Continuation of Families of Frozen Orbits in the Zonal Problem of Artificial Satellite Theory," *Celestial Mechanics and Dynamical Astronomy*, Vol. 62, No. 2, 1995, pp. 167–181. doi:10.1007/BF00692085

[10] Coffey, S. L., Deprit, A., and Deprit, E., "Frozen Orbits for Satellites Close to an Earth-Like Planet," *Celestial Mechanics and Dynamical Astronomy*, Vol. 59, No. 1, 1994, pp. 32–72.doi:10.1007/BF00691970

[11] Coffey, S. L., Deprit, A., Deprit, E., and Healy, L., "Painting the Phase Space Portrait of an Integrable Dynamical System," *Science*, Vol. 247, Feb. 1990, pp. 833–836. doi:10.1126/science.247.4944.833

[12] Coffey, S. L., Deprit, A., and Miller, B. L., "The Critical Inclination in Artificial Satellite Theory," *Celestial Mechanics*, Vol. 39, No. 4, 1986, pp. 365–406. doi:10.1007/BF01230483

[13] San Juan, J. F., "MathATESAT: A Symbolic-Numeric Environment in Astrodynamics," University of La Rioja, Spain (in preparation).

[14] de Saedeleer, B., "Analytical Theory of a Lunar Artificial Satellite with Third Body Perturbations," *Celestial Mechanics and Dynamical Astronomy*, Vol. 95, Nos. 1–4, 2006, pp. 407–423. doi:10.1007/s10569-006-9029-6

[15] de Saedeleer, B., and Henrard, J., "The Combined Effect of J_2 and C_{22} on the Critical Inclination of a Lunar Orbiter," *Advances in Space Research*, Vol. 37, No. 1, 2006, pp. 80–87. doi:10.1016/j.asr.2005.06.052

[16] Deprit, A., and Henrard, J., "Natural Families of Periodic Orbits," *Astronomical Journal*, Vol. 72, No. 2, 1967, pp. 158–172. doi:10.1086/110212

[17] Danby, J. M. A., *Fundamentals of Celestial Mechanics*, Willman-Bell, Richmond, VA, 1988.

[18] Folta, D., and Quinn, D., "Lunar Frozen Orbits," *2006 AIAA/AAS Astrodynamics Specialist Conference*, AIAA Paper 2006-6749, 2006

[19] Ramanan, R. V., and Adimurthy, V., "An analysis of near-circular lunar mapping orbits", *Journal of Earth System Science*, Vol. 114, No. 6, 2005, pp. 619–626. doi:10.1007/BF02715946

[20] Brouwer, D., and Clemence, G. M., *Methods of Celestial Mechanics*, Academic Press, New York, 1961.

[21] Brouwer, D., "Solution of the Problem of Artificial Satellite Theory Without Drag," *Astronomical Journal*, Vol. 64, No. 11, 1959, pp. 378–397. doi:10.1086/107958

[22] Kozai, Y., "The Motion of a Close Earth Satellite," *Astronomical Journal*, Vol. 64, No. 11, 1959, pp. 367–377. doi:10.1086/107957

[23] Garfinkel, B., "An Improved Theory of Motion of an Artificial Satellite," *Astronomical Journal*, Vol. 69, No. 3, 1964, pp. 223–229. doi:10.1086/109260

[24] Hori, G., "Theory of General Perturbations with Unspecified Canonical Variables," *Publications Astronomical Society of Japan*, Vol. 18, No. 4, 1966, pp. 287–296.

[25] Deprit, A., "Canonical Transformations Depending on a Small Parameter," *Celestial Mechanics*, Vol. 1, No. 1, 1969, pp. 12–30. doi:10.1007/BF01230629

[26] Deprit, A., "L'Algèbre symbolique en Mécanique Céleste," *Dynamics, Ephemerides and Astrometry of the Solar System*, edited by S. Ferraz-Mello, B. Morando, and J.-E. Arlot, Kluwer, Dordrecht, The Netherlands, 1996, pp. 267–282.

[27] Abad, A., Elipe, A., Palacián, J., and San-Juan, J. F., "ATESAT: A Symbolic Processor for Artificial Satellite Theory," *Mathematics and Computers in Simulation*, Vol. 45, Nos. 5–6, 1998, pp. 497–510. doi:10.1016/S0378-4754(97)00125-0

[28] Meyer, K. R., and Hall, G. R., *Introduction to Hamiltonian Dynamical Systems and the N-Body Problem*, Applied Mathematical Sciences Series, Vol. 90, Springer–Verlag, New York, 1992.

[29] Deprit, A., "The Elimination of the Parallax in Satellite Theory," *Celestial Mechanics*, Vol. 24, 1981, pp. 111–153. doi:10.1007/BF01229192

[30] Deprit, A., and Miller, B., "Simplify or Perish," *Celestial Mechanics*, Vol. 45, Nos. 1–3, 1988, pp. 189–200. doi:10.1007/BF01229001

[31] Deprit, A., "Delaunay Normalisations," *Celestial Mechanics*, Vol. 26, No. 1, 1982, pp. 9–21. doi:10.1007/BF01233178